*Journal of Thermal Analysis and Calorimetry, Vol. 94 (2008) 3, 641–648*

# ADSORPTION AND POROSITY PROPERTIES OF PURE AND MODIFIED CARBON NANOTUBE SURFACES

*M. Błachnio, P. Staszczuk* and G. Grodzicka*

Department of Physicochemistry of Solid Surface, Chemistry Faculty, Maria Curie-Sklodowska University
Maria Curie-Skłodowska Sq. 3, 20-031 Lublin, Poland

Modified carbon multiwall nanotubes were prepared via the oxidation process by means of 65% nitric acid or ferric nitrate dissolved with 65% nitric acid. Using special thermogravimetry and sorptometry methods physicochemical properties of pure and modified nanotube surfaces were investigated. A numerical and analytical procedure for the evaluation of total heterogeneous properties on the basis of liquid thermodesorption from the sample surfaces under the quasi-equilibrium conditions are presented. The calculations of the fractal dimensions of carbon nanotubes using the sorptometry and thermogravimetry data is presented.

***Keywords:*** *carbon nanotube, thermogravimetry, sorptometry, fractal dimensions, total heterogeneity*

## Introduction

Carbon nanotubes contain impurity admixtures immediately after synthesis without the purification stage. These are carbon nanoparticles, amorphous carbon and catalyst nanoparticles [1, 2]. Moreover most nanotubes as a direct product of synthesis are closed to a large extent with globular or polyhedral copulas which makes adsorption or capillarity in pores in internal walls of graphene layers and in the core itself impossible [3, 4]. Application of various techniques of carbon nanotube termination removal increases their adsorption properties due to accessibility of their internal space. Nanotubes occur as aggregates of single disordered nanotubes or bundles of large spatial order which allows adsorption in the spaces among nanotubes.

Carbon nanotube structure exhibits the presence of defects of chemical or structural character [5, 6]. Chemical defects occur in the form of heteroatoms replacing carbon atoms or attached to nanotube walls. Structural defects occur in the form of pentagons or heptagons in the hexagonal, graphene structure of nanotubes. Isolated heterocyclic rings impose positive or negative curvatures in the flat graphene layers resulting in the presence of inflexion and acute angles in the nanotube structures. On the surfaces of large curvature, the carbon-carbon bonds on the edges of regular pentagons or heptagons are subjected to large stresses and as a result undergo chemical reactions readily.

The paper presents the evaluation of adsorption properties and porosity of pure and modified carbon nanotube surfaces. Nitric acid as well as nitric acid and iron nitrate mixture were used as a modifier. Very precise instruments and measuring techniques were necessary to study the structure of nanometric size objects. The complex research methods used were sorptomatic measurements, liquid thermodesorption under the quasi-static conditions as well as AFM microscopy [7].

## Experimental

### *Materials*

Carbon multiwall nanotubes (Sample S1) *OD*= 30–50 nm, *ID*=5–15 nm, *l*=0.5–500 μm produced by Sigma–Aldrich (AFM picture is presented in Fig. 1) were modified by means of 65% nitric acid (Sample S2) or iron(III) nitrate dissolved with 65% nitric acid (Sample S3).

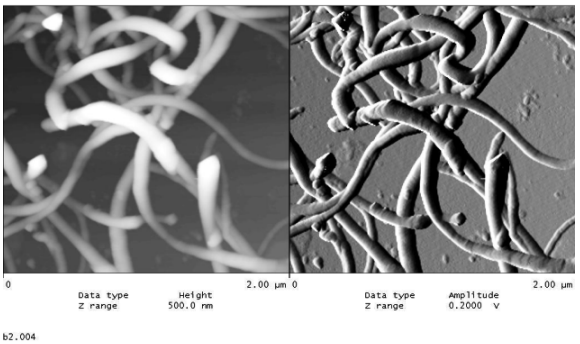


**Fig. 1** AFM photos of S1 sample

* Author for correspondence: piotrs@hektor.umcs.lublin.pl

*1388–6150/$20.00*

*Akadémiai Kiadó, Budapest, Hungary*
*Springer, Dordrecht, The Netherlands*

Modification I. A round-bottomed flask containing a sample of closed nanotubes (0.8 g) and nitric acid (65%; ca. 200 $cm^3$) was heated to reflux for 12 h. The nitric acid solution was decanted off, and the black sludge was pipetted onto glass filter paper. The sample was dried overnight in an oven at 60°C.

Modification II. A round-bottomed flask containing a sample of closed nanotubes (0.5 g), nitric acid (65%; ca. 100 $cm^3$) and iron(III) nitrate (ca. 1 g) was heated to reflux for 12 h. The nitric acid solution was decanted off, and the black sludge was pipetted onto glass filter paper. The sample was dried overnight in an oven at 60°C, and then calcinated by heating in a stream of argon at 450°C for 5 h for conversion of the iron(III) nitrate to the iron(III) oxide.

Empty core of the carbon nanotube can be filled with atoms or molecules of foreign substance in the form of separate molecules or continuous filaments [8]. To this end carbon nanotubes were heated in the solution of acid enriched with metal salts. The molecules of oxidizing acid while attacking the carbon-carbon bonds in the most curved sites of the couple closing the nanotube cause its detachment and penetration of iron(III) nitrate into the nanotube. Then the carbon nanotubes were subjected to high-temperature heating in argon atmosphere obtaining isolated metal oxide molecules arranged along their axes. During nanotubes oxidation by means of acid the nanomaterial surface was covered with the functional carboxylic, carbonyl and hydroxyl groups. These groups constitute centres for physicochemical phenomena or chemical reactions.

### *Methods*

Adsorption of apolar (benzene and *n*-octane) and polar (water and *n*-butanol) liquid layers was measured using the derivatograph Q-1500 D (MOM, Hungary) [9]. The samples were saturated with liquid vapours in the vacuum desiccator at $p/p_0$=1. The Q-TG mass loss and Q-DTG differential mass loss curves were measured under the quasi-isothermal conditions in the temperature range 20–250°C at a heating rate of 6° $min^{-1}$.

Porosity properties e.g. specific surface areas, pore size distribution and pore volume were calculated from low-temperature nitrogen adsorption-desorption isotherms measured by means of the Sorptomat ASAP 2405 V1.01 (Micrometrics Co., USA). AFM pictures were made by means of atomic force microscope (AFM) of NanoScope III type produced by Digital Instruments (USA).

## Results and discussion

Gas adsorption on the surface and in carbon nanotube pore spaces includes mass and energetic interactions between the adsorbent and adsorbate. The isotherms of nitrogen on carbon nanotubes presented in Fig. 2 can be

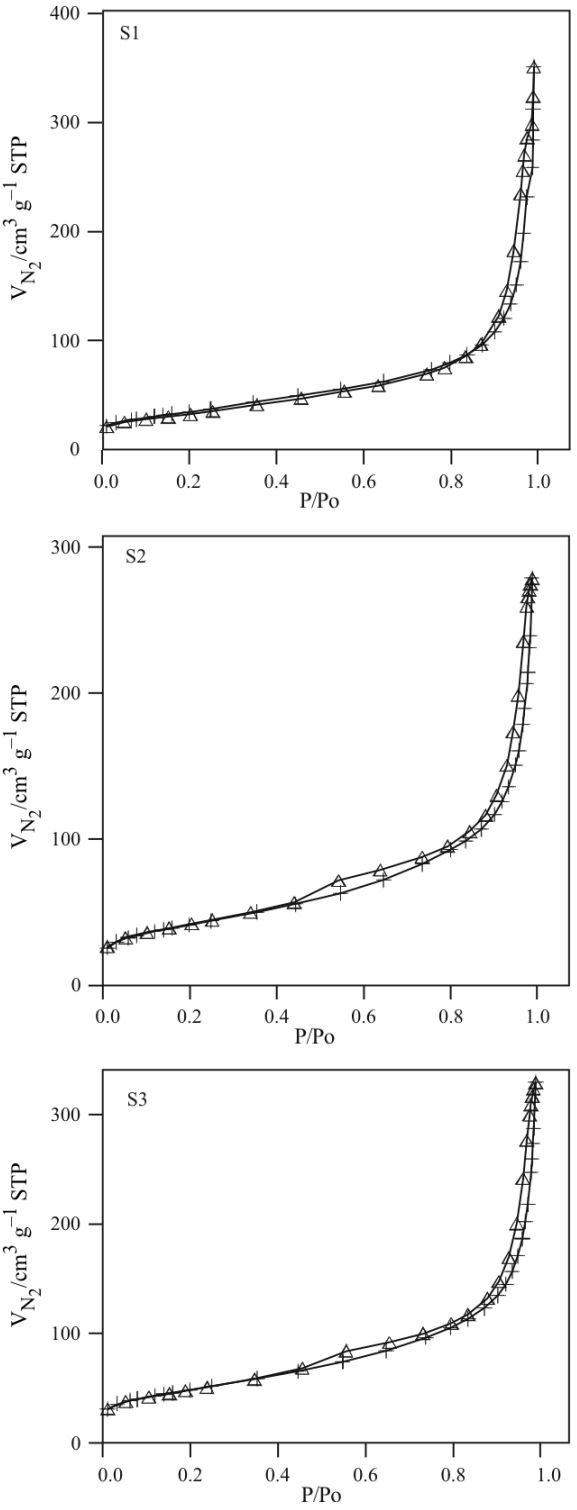


**Fig. 2** Isotherms of nitrogen adsorption and desorption for samples S1, S2 and S3

classified as type II according to BET. This type of isotherm describes the process of physical adsorption of nitrogen on the adsorbent surface. With the increase of adsorbate concentration in the gaseous phase, filling of pores of larger and larger diameters took place and a multimolecular adsorption layer was formed.

The isotherms (Fig. 2) can be divided into parts showing a multimolecular adsorption process. Part I of the isotherm is characterized by slow increase in the amount of adsorbed nitrogen and describes the surface adsorption process–monolayer formation. Parts II and III of the isotherm show the hysteresis loop connected with the capillary condensation process in mesopores but not very distinctly. Part II corresponds to capillary condensation at average values of relative pressure in small mesopores whose sizes correspond to the diameters of internal cores of nanotubes. In the case of unmodified nanotubes (sample S1) this part of isotherm is not observed which proves that nanotubes were closed at the ends and were not accessible to adsorbate molecules. Part III corresponds to capillary condensation at high values of relative pressure due to capillary condensation in pores of larger sizes. Pore size corresponding to this process is attributed to pores of aggregate structure. Individual nanotubes of different diameters and orientations interact through intermolecular forces forming an aggregate structure. Confined spaces among individual nanotubes are aggregate pores. Due to wide pore distribution and large volume, aggregate pores in carbon nanotubes have larger contribution into the capillary condensation process than the interior cavities of nanotubes.

Characterization of nanomaterial microporosity could be made by isotherms if the values $p/p_0$ were ultra-low (below 0.01). As the applied conditions of relative pressure of nitrogen vapours were insufficiently low, the obtained isotherms could be used only for determination of mesoporosity. To determine the parameters of microporosity i.e. the specific surface area and micropore volume, the method elaborated by Lippens and de Boer was used. Microporosity results from exterior and interior microporous cavities of nanotube surfaces.

The parameters describing the adsorbent structure determined from the sorptomatic investigations are the specific surface area ($S$), total pore volume ($V$), average pore diameter ($D$) (Table 1) with pore volume

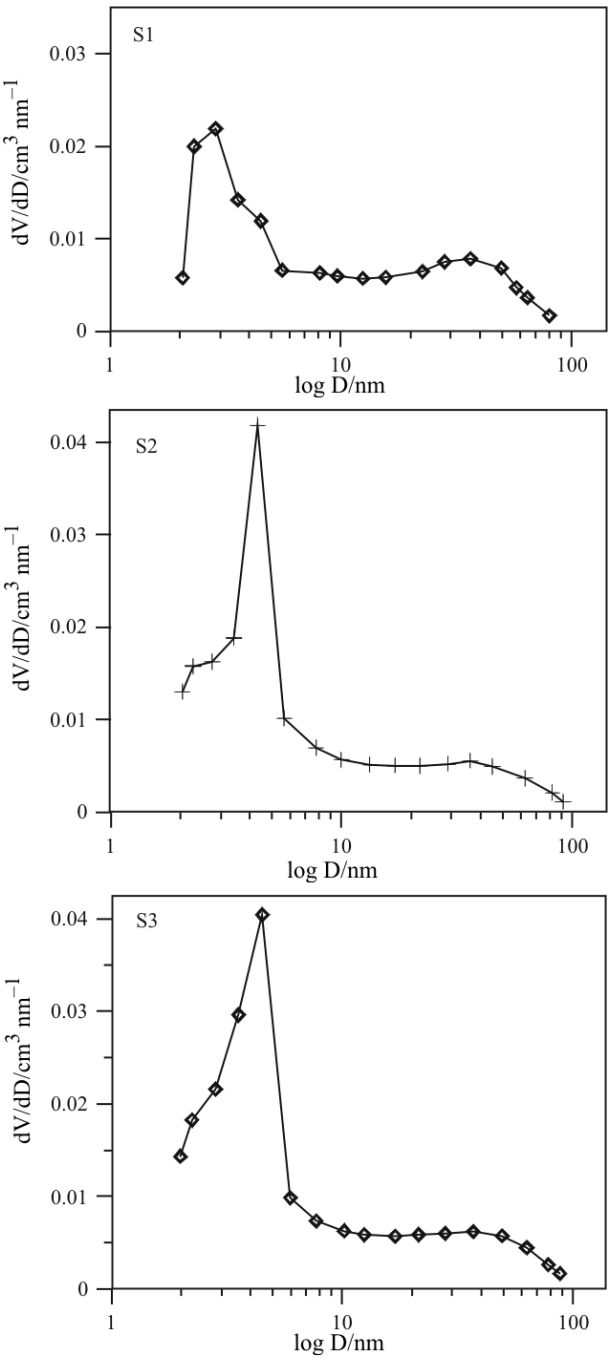


**Fig. 3** Pore size distribution functions of samples S1, S2 and S3

**Table 1** Change of adsorption-structural parameters of carbon nanomaterials

| Sample | $S_{BET}$/ m$^2$ g$^{-1}$ | $S_{MICRO}$/ m$^2$ g$^{-1}$ | $V_{(ads)BJH}$/ cm$^3$ g$^{-1}$ | $V_{(des)BJH}$/ cm$^3$ g$^{-1}$ | $V_{MICRO}$/ cm$^3$ g$^{-1}$ | $D_{AV}$/ nm |
|---|---|---|---|---|---|---|
| S1 | 122.2 | 7.58 | 0.55 | 0.54 | 0.003 | 13.1 |
| S2 | 146.4 | 16.39 | 0.44 | 0.42 | 0.007 | 9.05 |
| S3 | 171.5 | 23.02 | 0.52 | 0.50 | 0.010 | 9.36 |

distribution in relation to their diameters d$V$/d$D$=$f$($D$) (Fig. 3). The studies showed significant effect of modification on structural parameters of materials. Treating with acid increased two times the micropore surfaces. In the case of sample S3 the size of micropore surfaces increased three times. Increase of sample microporosity can be accounted for by accessibility of nanotube interior as well as by appearance of areas with damaged exterior graphene layers formed in the stage of boiling in strong oxidizing acid.

The total surface area of nanotubes increased from 122 to 146 $m^2$ $g^{-1}$ after modification with acid and 171 $m^2$ $g^{-1}$ after treating the sample with the acid and iron nitrate mixture. The increase of specific surface area resulted in reduction of average pore diameter from 13 to 9 and 9.4 nm due to appearance of functional groups and increase in intermolecular interactions in inter- and intragrain spaces of nanotube structures.

The functions of pore volume distribution confirm that the materials under investigations can be included into mesoporous adsorbents with the presence of additional micropores and macropores. The curves are bimodal of the Gaussian type with a sharp peak whose maximum corresponds to the diameter sizes 3, 4 and 5 nm for the samples S1, S2 and S3 respectively and with a soft peak with the maximum corresponding to the diameters 40 nm in all studied samples. The diameters of pores of such sizes have the largest contribution in sample porosity.

For cognitive reasons the samples were saturated with organic and inorganic substances in the diffusion process from the gaseous phase in vacuum desiccators. The liquids applied were water, *n*-butanol, benzene and *n*-octane. Penetration of liquid vapour molecules inside nanotubes takes place through the pentagonal ends or surface defects in the form of coupled pairs: pentagonal ring/heptagonal ring.

The Q-DTG curves (Figs 4 and 5) obtained from the studies of thermodesorption of the above mentioned liquids describe the energetic state of their molecules in intra- and intergrain pores of carbon material structure and in interior pores of carbon nanotubes. Energy of interactions among molecules

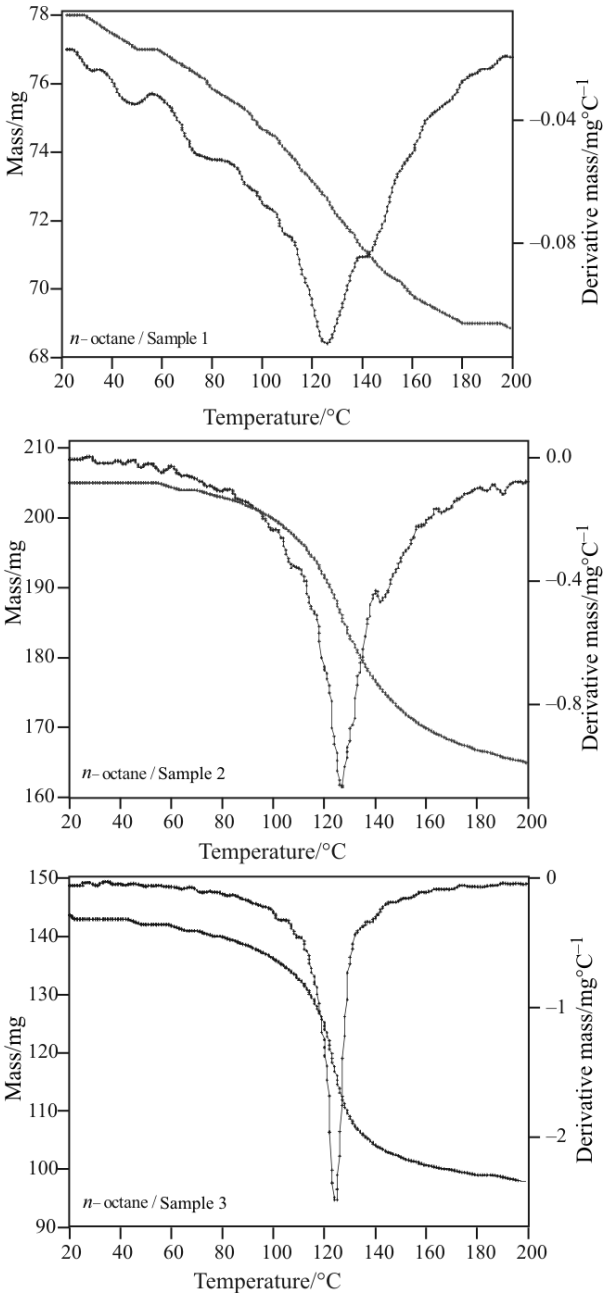


**Fig. 4** Thermodesorption of n-octane from the studied sample surfaces under the quasi-static conditions

**Table 2** Adsorption parameters evaluated on the base of the liquid thermodesorption from nanomaterial surfaces

| Parameter | Water | | | *n*-Octane | | | *n*-Butanol | | | Benzene | | |
|---|---|---|---|---|---|---|---|---|---|---|---|---|
| | S1 | S2 | S3 | S1 | S2 | S3 | S1 | S2 | S3 | S1 | S2 | S3 |
| $a$/mg $mg^{-1}$ | 0.08 | 0.57 | 0.70 | 0.16 | 0.32 | 0.55 | 0.44 | 0.72 | 1.00 | 0.53 | 0.81 | 1.22 |
| $n$/mmol $g^{-1}$ | 4.28 | 31.55 | 38.85 | 1.38 | 2.79 | 4.84 | 5.99 | 9.68 | 13.49 | 6.81 | 10.42 | 15.66 |
| θ/mmol $m^{-2}$ | 0.03 | 0.22 | 0.23 | 0.01 | 0.02 | 0.03 | 0.05 | 0.07 | 0.08 | 0.06 | 0.07 | 0.09 |
| $k$ | 2.63 | 16.22 | 17.06 | 2.87 | 4.85 | 7.19 | 10.46 | 14.09 | 16.77 | 11.76 | 15.00 | 19.25 |

$a$ – the amount of adsorbed liquid vapor for 1 mg of dry adsorbent/mg $mg^{-1}$; $n$ – the number of moles of adsorbed liquid vapor for 1 g of adsorbent/mmol $g^{-1}$; θ – the degree of adsorbent surface coverage/mmol $m^{-2}$; $k$ – the statistical number of liquid monolayers on the adsorbent surface

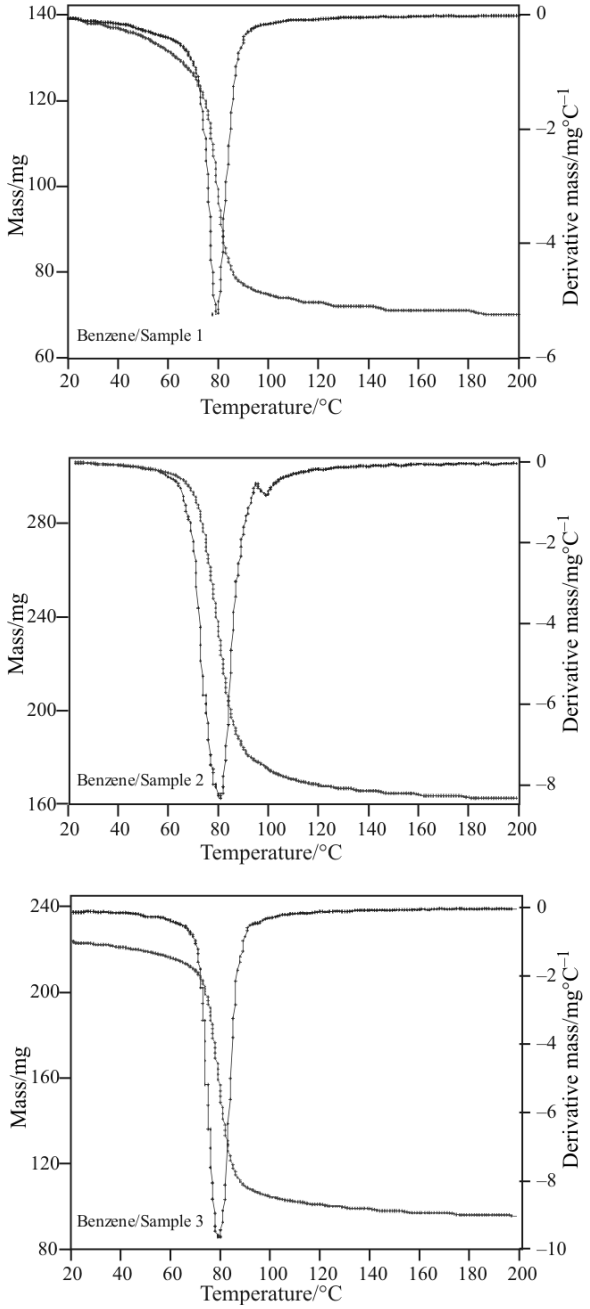


**Fig. 5** Thermodesorption of benzene from the studied sample surfaces under the quasi-static conditions

depends on the adsorbate type, properties of the surface on which they are adsorbed and sample porosity (presence of macro-, meso- and micropores). The differential Q-DTG curves are characterized by the presence of one distinct peak. This indicates continuity of the thermodesorption process and monotonic changes of adsorption layer properties depending on the distance of liquid molecules from the surface. In the case of water and *n*-octane thermodesorption from the sample S1, the obtained curve is in the form of broad band resulting from small amounts of vapours of the

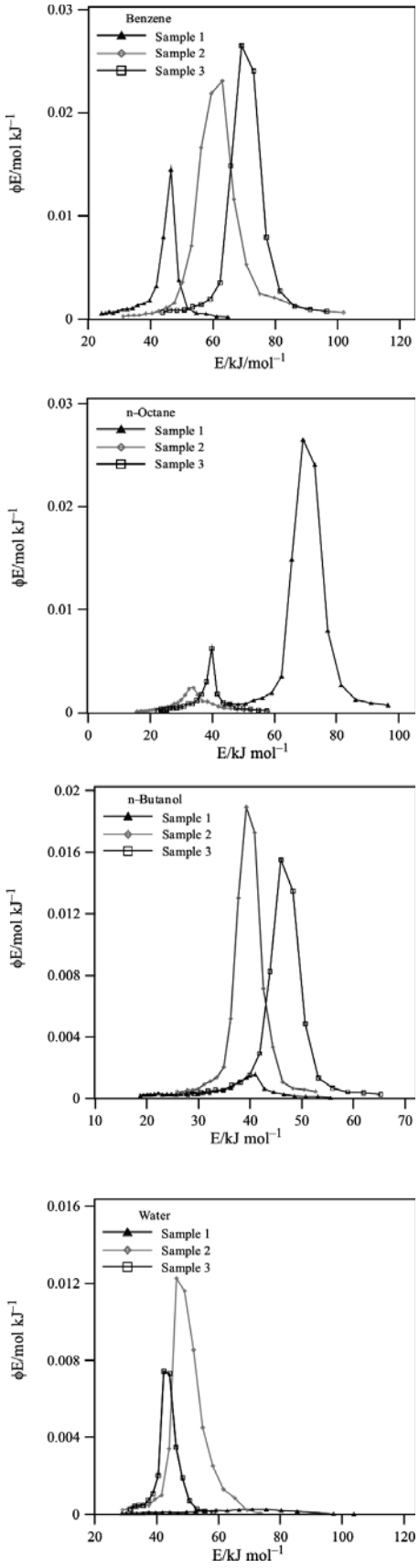


**Fig. 6** Curves of benzene, *n*-octane, *n*-butanol and water desorption energy distribution from the samples

liquids adsorbed on the sample S1 and large differentiation of the energetic system.

Interpretation of the thermodesorption curves also consists in determination of the amount of liquid bounded in the form of adsorption layer, adsorption capacity of samples and statistical number of monolayers of individual liquids present on the sample surfaces (Table 2).

The amounts of adsorbed liquid vapours for 1 mg of dry adsorbent tend to increase in the direction S1<S2<S3 and the amounts of adsorbed vapours are in the decreasing order benzene>*n*-butanol>*n*-octane>water. Except for the sample S1, the calculated degrees of coverage of adsorbent surfaces are the largest for water. The sample modified with the mixture adsorbs the largest number of liquid monolayers but the initial sample the smallest numbers of monolayers.

The method of liquid thermodesorption was also used for calculation of desorption energy and presentation of the desorption energy distribution function in the graphic form (Fig. 6). The desorption energy distribution from the Q-TG and Q-DTG curves was derived using an equation for the desorption kinetics characterized by a constant value of the desorption energy [10, 11]:

$$-\frac{1}{1-\theta_i}\frac{d\theta_i}{dT}=\frac{\nu_i}{\beta}\exp\left(-\frac{E_i}{RT}\right) \quad (1)$$

where: $T=T_0+\beta t$, θ is the degree of surface coverage, ν is the entropy factor, $E_i$ is the desorption energy calculated for each temperature, $T_0$ and $T$ are the initial and given temperatures of desorption, respectively, β is the heating rate of the sample, $t$ is the time and $R$ is the universal gas constant.

The final expression for determination of desorption energy distribution ρ($E$) can be expressed in the form:

$$\rho(E)=-\frac{d\theta}{dT}\frac{1}{T} \quad (2)$$

This function enables estimation of energetic heterogeneity of sorbent surface as it is the derivative a number of active centres on the surface in relation to the desorption energy. The energy distribution functions differ in values (Table 3) which indicates a complex mechanism of desorption process as well as the effect of modification. The higher the values of distribution function, the more active centres of a given energy on the solid surface. The increase in the value $E_d$ indicates the increase in adsorbent-adsorbate interactions. The determined values of *n*-octane and water desorption energy are reduced for the modified samples compared with the initial sample. For benzene and *n*-butanol a reverse dependence is observed. The shape of desorption energy distribution function curves is similar to the Gaussian curves with one distinct peak indicating existence of one main active centre on the surface of adsorbents. Broadening of bands on the curves of desorption energy distribution points to the increase in energetic heterogeneity of the studied material. This is most evident for the curves of desorption energy distribution for the S1/*n*-octane, S2/benzene, *n*-butanol and water, S3/benzene and *n*-butanol sample system.

Structural characterization of carbon nanomaterials was made from the determined surface and volumetric fractal coefficients from the data of thermogravimetric and sorptomatic methods used independently (Table 4). The description of the analytical method for surface fractal coefficients from the liquid thermodesorption data is given in [12]. The main equation is of the form:

$$D_f=(2+3n_f)/(1+n_f) \quad (3)$$

Volumetric fractal coefficients were calculated using the method based on the theory of Frenkel,

**Table 3** Comparison of desorption energy ranges for individual materials

| Sample | Benzene | | *n*-Octane | | *n*-Butanol | | Water | |
|---|---|---|---|---|---|---|---|---|
| | $\Delta E_d$ | $E_{d_{max}}$ | $\Delta E_d$ | $E_{d_{max}}$ | $\Delta E_d$ | $E_{d_{max}}$ | $\Delta E_d$ | $E_{d_{max}}$ |
| S1 | 40 | 46 | 30 | 70 | 37 | 41 | 75 | 68 |
| S2 | 71 | 63 | 42 | 34 | 26 | 39 | 45 | 46 |
| S3 | 53 | 69 | 35 | 40 | 35 | 46 | 26 | 42 |

**Table 4** Values of the volumetric and surface fractal coefficients

| Sample | Sorptometric method | | | | Thermogravimetric method | | | | |
|---|---|---|---|---|---|---|---|---|---|
| | Eq. (4) | Eq. (5) | Eq. (6) | Average | Water | *n*-Butanol | Benzene | *n*-Octane | Average |
| S1 | 2.56 | 2.51 | 2.41 | 2.49 | 2.51 | 2.50 | 2.52 | 2.52 | 2.51 |
| S2 | 2.61 | 2.44 | 2.73 | 2.59 | 2.53 | 2.50 | 2.50 | 2.53 | 2.52 |
| S3 | 2.62 | 2.43 | 2.75 | 2.60 | 2.56 | 2.50 | 2.53 | 2.55 | 2.54 |

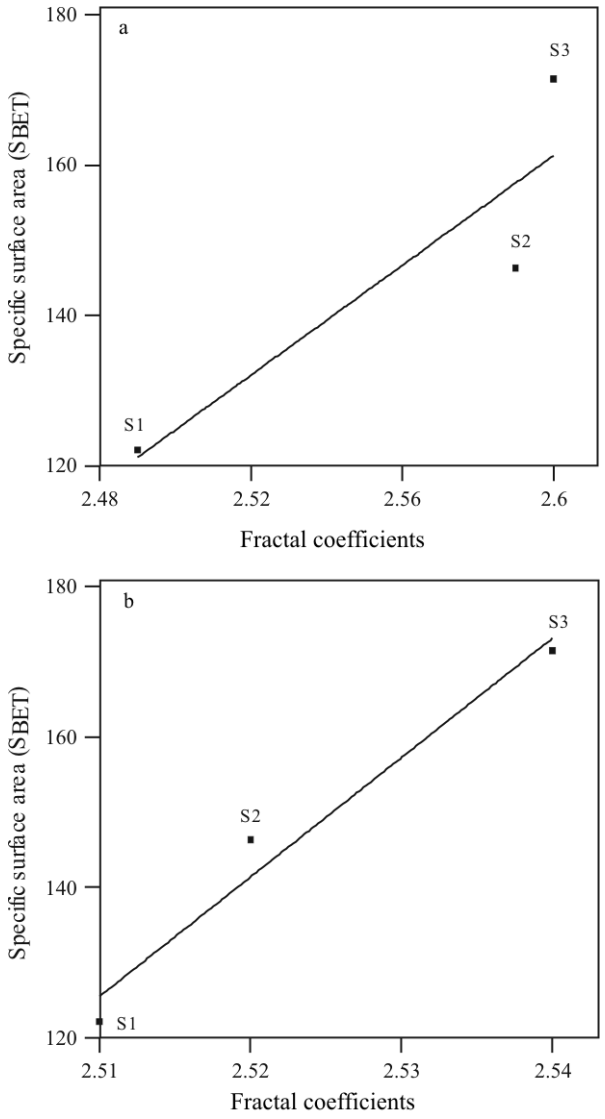


**Fig. 7** The dependences of specific surface areas and fractal coefficients calculated from a – sorptomatic and b –thermogravimetric methods (right side) of materials

Halsey, Hill and Kisielev from the following equations [13–16]:

$$D_f=2+n_f \quad (4)$$

$$D_f=3-\mathrm{d}[\ln a(x)]/\mathrm{d}[\ln(-\ln x)] \quad (5)$$

$$D_f=2+\mathrm{d}[\ln\int(-\ln x)\mathrm{d}a]/\mathrm{d}[\ln(-\ln x)] \quad (6)$$

where $n_f$ is a fractional part of the fractal, $a$ is the size of adsorption, $x$ is the segment of experimental isotherm.

The average values of volumetric fractal coefficients change in the range of 2.49–2.60 evidencing the differences in pore distribution. The more intensive modification was applied to the structure of initial sample surface, the greater the values of volumetric fractal coefficients were. The surface fractal coefficients change in the range of 2.51–2.54 which results from similar values of specific surface areas of these materials. The obtained values of porous and surface fractal coefficients are comparable and indicate well developed surfaces as well as a wide range of pore distribution in the nanomaterials under investigation. This is confirmed by the sizes of specific surface areas and pore distributions according to the sizes of studied nanomaterials determined from sorptomatic measurements.

Figure 7 presents relationships between specific surface areas and fractal coefficients calculated from sorptometry and thermogravimetric methods of studied nanomaterials. From the above Fig. it appears that bigger fractal coefficients have been obtained for bigger surface areas of surface studied.

## Conclusions

Studies of low-temperature nitrogen adsorption on pure and modified carbon nanotubes showed the effect of modification on changes in the porous structure of studied materials. Increase in specific surface area results from microporosity development which can be explained by nanotube interior accessibility as well as appearance of areas with damaged exterior graphene layers of the sizes corresponding to micropores. Carbon nanotubes treatment with acid resulted in appearance of functional groups on the surface, which constitute centres for intermolecular interactions in intra- and intergrain spaces of nanotube structures. Due to the increase of intermolecular interactions, the increase of nanotubes aggregation and the reduction of pores volume in mesopores were observed.

The shape of Q-TG curves loss in liquid thermodesorption from the samples is characterized by single step, which indicates monotonic (continuous) changes of properties of liquid adsorption layers adsorbed on the surface of carbon nanotubes. The presence of single inflexions on the Q-TG curves results from the determined bonding energy of liquid molecules with the surface of studied sample as well as in adsorption layers. The differential mass loss curves Q-DTG describe the kinetics of thermodesorption of studied liquids from carbon nanomaterial surface. They are characterized by a distinct peak, which is associated with evaporation of liquid molecules being in similar energetic states in the adsorption layer.

The surface properties from the thermal analysis data were determined by means of the analytical-numerical method. Desorption energies and desorption energy distribution functions were calculated from the Q-TG and Q-DTG data. The shape of thermodesorption energy distribution function curves is of the Gaussian type with one evident peak.

The fractal coefficients were calculated from the thermal analysis and sorptomatic data. They can be

used as additional parameters to estimate geometric heterogeneity of solid surfaces. The obtained values are the evidence of porous structure of pure and modified carbon nanotubes.

## References


1 J. Zhijie, W. Zhengyuan, L. Ji, W. Bingqing and W. Dehai, Carbon, 37 (1999) 903.
2 Z. W. Pan, S. S. Xie, B. H. Chang, L. F. Sun, W. Y. Zhou and G. Wang, Chem. Phys. Lett., 299 (1999) 97.
3 L. Kin-tak, S. San-Qiang and Ch. Hui-ming, Compos. Sci. Technol., 63 (2003) 1162.
4 Y. Quan-Hong, H. Peng-Xiang, B. Shuo, W. Mao-Zhang and Ch. Hui-Ming, Chem. Phys. Lett., 345 (2001) 19.
5 S. Q. Feng, D. P. Yu, G. Hu, X. F. Zhang and Z. J. Zhang, J. Phys. Chem., 58 (1997) 1887.
6 Ch. Singh, M. S. P. Shaffer and A. H. Windle, Carbon, 41 (2003) 2359.
7 P. Staszczuk, Handbook of Thermal Analysis and Calorimetry, (M. E. Brown and P. K. Gallagher, Eds), Volume 5: Recent Advances, Techniques and Applications, Chapter 10, pp. 343–392, Elsevier, Oxford, UK 2008.
8 D. Ugarte, T. Stöckli, J. M. Bonard, A. Châtelain and W. A. de Heer, Appl. Phys. A: Mat. Sci. Proc., 67 (1998) 101.
9 F. Paulik, Special Trends in Thermal Analysis, J. Wiley and Sons Ltd., Chichester, England 1995.
10 P. Staszczuk, D. Sternik and V.V. Kutarow, J. Therm. Anal. Cal., 69 (2002) 23.
11 P. Staszczuk, V. V. Kutarow and M. Płanda, J. Therm. Anal. Cal., 71 (2003) 445.
12 P. Staszczuk, J. C. Bazan, M. Błachnio, D. Sternik and N. J. Garcia, J. Therm. Anal. Cal., 86 (2006) 61.
13 B. M. Kats and V. V. Kutarov, Langmuir, 12 (1996) 2762.
14 P. Pfeifer, Fractals in Physics, Amsterdam, Holland, 1986.
15 P. Staszczuk, J. Therm. Anal. Cal., 79 (2005) 545.
16 P. Staszczuk, M. Błachnio, E. Kowalska and D. Sternik, J. Therm. Anal. Cal., 86 (2006) 51.


DOI: 10.1007/s10973-008-9371-x